

Drosophila FMRP participates in the DNA damage response by regulating G2/M cell cycle checkpoint and apoptosis

Wei Liu¹, Fangfang Jiang^{1,†}, Xiaolin Bi^{2,3,*} and Yong Q. Zhang^{1,*}

¹Key Laboratory for Molecular and Developmental Biology, Institute of Genetics and Developmental Biology, Chinese Academy of Sciences, Beijing 100101, People's Republic of China, ²Institute of Cancer Stem Cell, Dalian Medical University, Dalian 116044, People's Republic of China, and ³Key Laboratory for Biological Effects of Nanomaterials and Nanosafety, Institute of High Energy Physics, Chinese Academy of Sciences, Beijing 100049, People's Republic of China

Received June 1, 2012; Revised June 1, 2012; Accepted July 23, 2012

Fragile X syndrome, the most common form of inherited mental retardation, is caused by the loss of the fragile X mental retardation protein (FMRP). FMRP is a ubiquitously expressed, multi-domain RNA-binding protein, but its *in vivo* function remains poorly understood. Recent studies have shown that FMRP participates in cell cycle control during development. Here, we used *Drosophila* mutants to test if FMRP plays a role in DNA damage response under genotoxic stress. We found significantly fewer *dfmr1* mutants survived to adulthood than wild-types following irradiation or exposure to chemical mutagens, demonstrating that the loss of *drosophila* FMRP (dFMRP) results in hypersensitivity to genotoxic stress. Genotoxic stress significantly reduced mitotic cells in wild-type brains, indicating the activation of a DNA damage-induced G2/M checkpoint, while mitosis was only moderately suppressed in *dfmr1* mutants. Elevated expression of cyclin B, a protein critical for the G2 to M transition, was observed in the larval brains of *dfmr1* mutants. *CycB* mRNA transcripts were enriched in the dFMRP-containing complex, suggesting that dFMRP regulates DNA damage-induced G2/M checkpoint by repressing *CycB* mRNA translation. Reducing *CycB* dose by half in *dfmr1* mutants rescued the defective G2/M checkpoint and reversed hypersensitivity to genotoxic stress. In addition, *dfmr1* mutants exhibited more DNA breaks and elevated p53-dependent apoptosis following irradiation. Moreover, a loss-of-heterozygosity assay showed decreased irradiation-induced genome stability in *dfmr1* mutants. Thus, dFMRP maintains genome stability under genotoxic stress and regulates the G2/M DNA damage checkpoint by suppressing *CycB* expression.

INTRODUCTION

Fragile X syndrome (FXS), the most common form of inherited mental retardation, is caused by transcriptional silencing of *fragile X mental retardation 1 (FMR1)* gene (1). *FMR1* encodes a ubiquitously expressed, multiple domain RNA-binding protein FMRP (fragile X mental retardation protein). Although it was identified three decades ago, the *in vivo* functions of FMRP remain poorly understood.

Emerging evidence supports that FMRP is critical for the differentiation and proliferation of germline and neural stem cells. Studies with neurospheres generated from the brains of *Fmr1* knock-out mice and Fragile X fetus show that the loss of FMRP leads to an increased number of neurons but a reduced number of glial cells (2). More recently, Luo *et al.* (3) showed increased proliferation and altered fate specification of adult neural stem cells in the *Fmr1* knockout mice. They further showed that FMRP regulates the translation

*To whom correspondence should be addressed. Tel: +86 1064807611; Fax: +86 1064807611; Email: yqzhang@genetics.ac.cn (Y.Q.Z.); Tel: +86 41186110150; Fax: +86 41186110150; Email: bixl@dlmedu.edu.cn (X.B.)

[†]Present address: Ben May Department for Cancer Research, University of Chicago, Chicago, IL 60637, USA.

of several factors involved in stem cell proliferation and differentiation, including cyclin D1, cyclin-dependent kinase 4 (CDK4) and glycogen synthase kinase 3 β (3). In *Drosophila*, drosophila FMRP (dFMRP) collaborates with caprin, a translational regulator, to regulate cell cycle progression by repressing the expression of *CycB* during embryo development (4). In the developing ovary, *dfmr1* mutants display defective germline proliferation and cell cycle progression (5,6), while in the larval brain, *dfmr1* mutations lead to a significant increase in the number of mitotic neuroblasts (7). In addition, a single neuroblast from *dfmr1* mutants generates significantly more neurons than wild-type controls (7). The altered differentiation and proliferation of germline and neural stem cells in FMRP-deficient mammals and *dfmr1* mutant *Drosophila* together suggest that FMRP may be involved in cell cycle control.

The molecular pathways for cell cycle control, like those involved in DNA repair and apoptosis, are activated in response to DNA damage (8). When DNA damage occurs in G2 phase, the CycB-CDK1 complex is inactivated, leading to cell cycle arrest at the G2 to M transition (9). In the HeLa cells, DNA damage causes a transient decrease in *CycB* expression at both the transcriptional and translational levels (10,11). Overexpression of CycB abrogates DNA damage-induced G2 arrest, whereas a reduction in CycB1 prolongs G2 phase in HeLa cells after irradiation (12). Thus, the CycB-CDK1 complex acts as a critical regulator at the G2/M transition in cells with DNA damage.

Both the DNA damage response pathways and FMRP are highly conserved across evolution (13–15). Hence, it is possible to investigate their roles in *Drosophila*. In this study, we found that *Drosophila dfmr1* null mutants were hypersensitive to genotoxic stress. Loss of *dfmr1* caused a defective G2/M cell cycle checkpoint following DNA damage, leading to excessive mitosis in association with the elevated expression of CycB. *CycB* mRNA was enriched in the dFMRP-containing protein complexes from larval brains, suggesting a negative regulation of CycB by *dfmr1*. In addition, *dfmr1* mutants showed excessive apoptosis, more DNA breaks and decreased genome stability upon DNA damage. Collectively, our data demonstrate for the first time that dFMRP regulates the DNA damage response by suppressing *CycB* expression and inhibiting apoptosis.

RESULTS

dfmr1 mutants are hypersensitive to genotoxic stress

Mounting evidence indicates that FMRP plays a role in cell cycle control (3–7). As the cell cycle is tightly linked to DNA damage response, we examined the sensitivity of *dfmr1* mutants to ionizing radiation which causes a wide spectrum of DNA defects including DNA double-strand breaks (DSBs). The wandering third-instar larvae were exposed to γ -ray radiation at different doses. In both wild-type and homozygous *dfmr1*^{50M} null mutants, the irradiation of larvae caused a dose-dependent decrease in adult survival (Fig. 1). However, *dfmr1* mutants were more sensitive compared with the *w*¹¹¹⁸ controls to irradiation at all doses used (Fig. 1). At a dose of 40 Gy, only a few *dfmr1* mutants survived ($1.7 \pm 1.3\%$, $n = 180$),

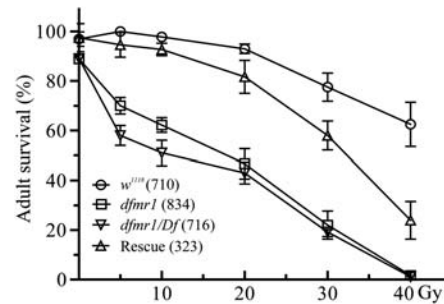


Figure 1. *dfmr1* mutants were hypersensitive to irradiation. Third-instar larvae were exposed to γ -ray radiation at 0, 5, 10, 20, 30 and 40 Gy. Surviving adults were counted 1 week after the treatment. The percentage of surviving *dfmr1* adults against the total number of larvae irradiated was calculated for each genotype. Homozygous *dfmr1*^{50M} mutants exhibited significantly higher lethality than wild types at all doses tested. *dfmr1*^{50M}/*Df*(3*R*)*BSC38* hemizygous mutants displayed similar hypersensitivity to irradiation as *dfmr1*^{50M} homozygous mutants, whereas one copy of the genomic *dfmr1* transgene (*Pf**w*⁺:*dfmr1*)/+ largely reversed the hypersensitivity of *dfmr1*^{50M} homozygous mutants. At least 50 larvae of each genotype were treated at each dose and three independent experiments were conducted. The total number of larvae tested for each genotype is indicated in the parenthesis. Error bars indicate SEM.

whereas more than half of the irradiated *w*¹¹¹⁸ larvae survived to adults ($62.5 \pm 8.9\%$, $n = 160$). The *dfmr1*^{50M} hemizygotes [*dfmr1*^{50M}/*Df*(3*R*)*BSC38*] showed hypersensitivity to irradiation similar to the *dfmr1*^{50M} homozygous mutants (Fig. 1), whereas one copy of the wild-type genomic *dfmr1* transgene partially reversed the hypersensitivity to irradiation (Fig. 1). The partial rescue is not caused by a background mutation on the *dfmr1*^{50M} chromosome but likely by the fact that the genomic transgene does not faithfully mimic the expression pattern of the endogenous protein (16). These results demonstrate that the hypersensitivity to irradiation is specifically caused by *dfmr1* mutations.

To confirm the hypersensitivity of *dfmr1* mutants to irradiation, we treated the offspring of *dfmr1*^{50M} heterozygous parents with the mutagenic chemicals methyl methanesulfonate (MMS) and hydroxyurea (HU). MMS methylates DNA on N⁷-deoxyguanine and N³-deoxyadenine, resulting in DNA DSBs, whereas HU reduces the production of deoxyribonucleotides by inhibiting ribonucleotide reductase and thus stalls DNA replication (17). In the absence of mutagen treatment, *dfmr1*^{50M} homozygotes accounted for the expected one third of the total adults ($29.8 \pm 2.7\%$, Table 1). The treatment of larvae with MMS caused a dose-dependent reduction in the survival of *dfmr1*^{50M} homozygotes as indicated by the reduced fraction of homozygotes in the total surviving adult population. For example, the fraction of *dfmr1*^{50M} homozygotes at the adult stage was reduced from 29.8 ± 2.7 to $20.3 \pm 3.9\%$ in larvae treated with 0.05% MMS and to $5.6 \pm 2.0\%$ in larvae treated with 0.20% MMS (Table 1). HU treatment caused a similar effect; the fraction of *dfmr1*^{50M} homozygotes was reduced from 26.1 ± 3.3 to $15.1 \pm 4.0\%$ as the HU dose was increased from 2.5 to 7.5 μ M (Table 1). Thus, *dfmr1* mutants were hypersensitive to two forms of genotoxic stress, chemical mutagens and γ -ray radiation.

Table 1. Increased sensitivity of *dfmr1* mutants to chemical mutagens

| Agents | Concentrations | % homozygotes | SEM | <i>P</i> -value | <i>n</i> |
|--------|----------------|---------------|-----|-----------------|----------|
| MMS | 0.00‰ | 29.8 | 2.7 | NA | 426 |
| | 0.05‰ | 20.3 | 3.9 | <0.05 | 162 |
| | 0.10‰ | 16.2 | 1.0 | <0.01 | 241 |
| | 0.20‰ | 5.6 | 2.0 | <0.01 | 144 |
| HU | 0.0 μM | 29.8 | 2.7 | NA | 426 |
| | 2.5 μM | 26.1 | 3.3 | NS | 222 |
| | 5.0 μM | 18.0 | 4.2 | <0.05 | 200 |
| | 7.5 μM | 15.1 | 4.0 | <0.01 | 152 |

MMS, methyl methanesulfonate; HU, hydroxyurea; NA, not assayed; NS, not significant. The offspring scored were derived from a cross between heterozygous *dfmr1*^{50M}/*TM6B* parents. Percentages are the fraction of *dfmr1*^{50M} homozygotes to the total surviving adults indicated by *n*.

Defective G2/M checkpoint in *dfmr1* mutants

When the genome DNA is damaged, the cell cycle is arrested by signaling systems that act as checkpoints to allow enough time for the DNA repair (8,9,18). We hypothesized that the hypersensitivity to DNA damage in *dfmr1* mutants might result from a defective cell cycle checkpoint. To investigate this possibility, the brain lobes and ventral nerve cords from third-instar larvae of different genotypes were stained with the mitotic marker anti-phospho-Histone H3 (PH3) and the number of mitotic cells was quantified. We observed a 15.62% increase in the number of mitotic cells in the vehicle-treated *dfmr1*^{50M} brains (689.8 ± 28.3 , $n = 6$) compared with the wild-type (596.6 ± 61.6 , $n = 5$), although this difference was not statistically significant ($P > 0.05$; Fig. 2A1, B1 and D). Following HU treatment at 50 mg/ml for 5 h, there were few mitotic cells in the wild-type larval brains (90.3 ± 10.7 ; Fig. 2A2 and D), indicating an intact G2/M checkpoint in response to the DNA damage. In the HU-treated *dfmr1*^{50M} brains, however, the number of mitotic cells was 4.7-fold higher than the HU-treated controls (426.9 ± 44.8 ; $P < 0.001$; Fig. 2A2, B2 and D), indicating a defective G2/M DNA damage checkpoint in *dfmr1* mutants. *dfmr1*^{50M} hemizygotes [*dfmr1*^{50M}/*Df(3R)BSC38*] showed a G2/M checkpoint defect similar to the homozygous mutants (513.2 ± 18.8 ; Fig. 2D). Importantly, one copy of the wild-type genomic *dfmr1* transgene significantly rescued the increased number of mitotic cells in *dfmr1* mutant brains (332.5 ± 41.1 ; $P < 0.05$; Fig. 2D). The Mei-41 protein is the *Drosophila* homolog of the mammalian checkpoint kinase ataxia telangiectasia-mutated and rad-3-related (ATR), the principle regulator of the G2/M checkpoint upon DNA damage (19,20). As expected, the number of mitotic cells significantly increased in the brains of HU-treated strong loss-of-function *mei-41*^{RTI} mutants (566.7 ± 67.9 , $n = 6$; $P < 0.001$; Fig. 2C and D) compared with the wild-type.

The defective G2/M checkpoint was also observed in the wing discs of *dfmr1* mutants following irradiation. In the absence of irradiation, the number of mitotic cells detected by anti-PH3 staining in *dfmr1*^{50M} wing discs was comparable with the wild-type (Fig. 3A1, B1 and D). However, 1 h after irradiation at 40 Gy, the number of mitotic cells in *dfmr1*^{50M} wing discs was 3.1-fold higher than the wild-type (103.1 ± 44.8 for *dfmr1* mutants versus 32.9 ± 6.3 for wild-type; $P < 0.01$; Fig. 3A2, B2 and D), consistent with the increased level of

mitosis in HU-treated *dfmr1* brains (Fig. 2). As a positive control, *mei-41*^{RTI} wing discs showed a much larger number of mitotic cells following irradiation (314.5 ± 22.7 ; $P < 0.001$; Fig. 3C2 and D). The significantly increased number of mitotic cells in *dfmr1* mutants after HU treatment and irradiation (Figs 2 and 3) shows that dFMRP regulates G2/M checkpoint under genotoxic stress.

To verify the G2/M checkpoint defect in the HU-treated *dfmr1* mutant brains, we used flow cytometry to measure the cell cycle profile of larval brains. Wild-type brains from HU-treated flies showed an obvious 39.2% decrease in the percentage of cells in G2/M phases ($8.9 \pm 0.9\%$; Fig. 4A2) compared with the mock-treated wild-types ($14.7 \pm 0.7\%$; Fig. 4A1 and C). This is understandable, as HU-treatment led to a greatly reduced number of mitotic cells (Fig. 2). In contrast, there was a comparable fraction of cells in G2/M phases in HU-treated and mock-treated *dfmr1*^{50M} mutants ($10.7 \pm 1.1\%$ for HU-treated and $11.8 \pm 0.9\%$ for untreated mutants; Fig. 4B1, B2 and C). As a control, *mei-41*^{RTI} mutants showed a phenotype similar to that of *dfmr1* mutants; again there was no obvious decrease in the fraction of cells in the G2/M phases after HU-treatment compared with the mock-treated *mei-41* mutants ($10.1 \pm 0.3\%$ for HU-treated and $11.7 \pm 0.1\%$ for untreated *mei-41* mutants; Fig. 4C). Together, the immunostaining (Figs 2 and 3) and cell cycle analysis by flow cytometry (Fig. 4) provide complementary evidence supporting that the loss of *dfmr1* causes a defect in G2/M checkpoint induced by DNA damage.

To examine whether the *dfmr1* mutation causes a defect at G1/S and intra-S checkpoints, we performed BrdU incorporation experiments. Incorporation of BrdU was equally reduced in wild-type and *dfmr1* mutants after HU treatment (Supplementary Material, Fig. S1), indicating normal G1/S and intra-S DNA damage checkpoints in *dfmr1* mutants. Thus, we conclude that *dfmr1* primarily regulates the G2/M DNA damage checkpoint.

Up-regulation of CycB expression in *dfmr1* mutant brains

The transition from one cell cycle phase to another is tightly controlled by cyclin-CDK complexes. The CycB-CDK1 complex is essential for the transition from G2 to M phase and CycB expression peaks during late G2 and early mitosis (21,22). Upon DNA damage, both *CycB* transcription and protein levels are down-regulated for a short period of time (10,11). Conversely, the overexpression of *CycB* overcomes the G2/M arrest induced by DNA damage in HeLa cells (12). It is therefore possible that the G2/M checkpoint defect in *dfmr1* mutants might be mediated through misregulated *CycB* expression. Quantitative polymerase chain reaction (PCR) detected a similar level of *CycB* transcripts in the larval brains of *dfmr1*^{50M} mutants and wild-types (Supplementary Material, Fig. S2). Western analysis, however, showed that the CycB protein level was significantly increased in *dfmr1* brains by 1.6-fold of the wild-type ($P < 0.01$; Fig. 5A and B). Similarly, after HU treatment, there was a significantly higher level of CycB protein in *dfmr1* mutant brains than in the wild-type ($P < 0.05$; Fig. 5A and B). The level of CycB showed no obvious alterations in wild-type animals after HU treatment, so did the level of CycB in

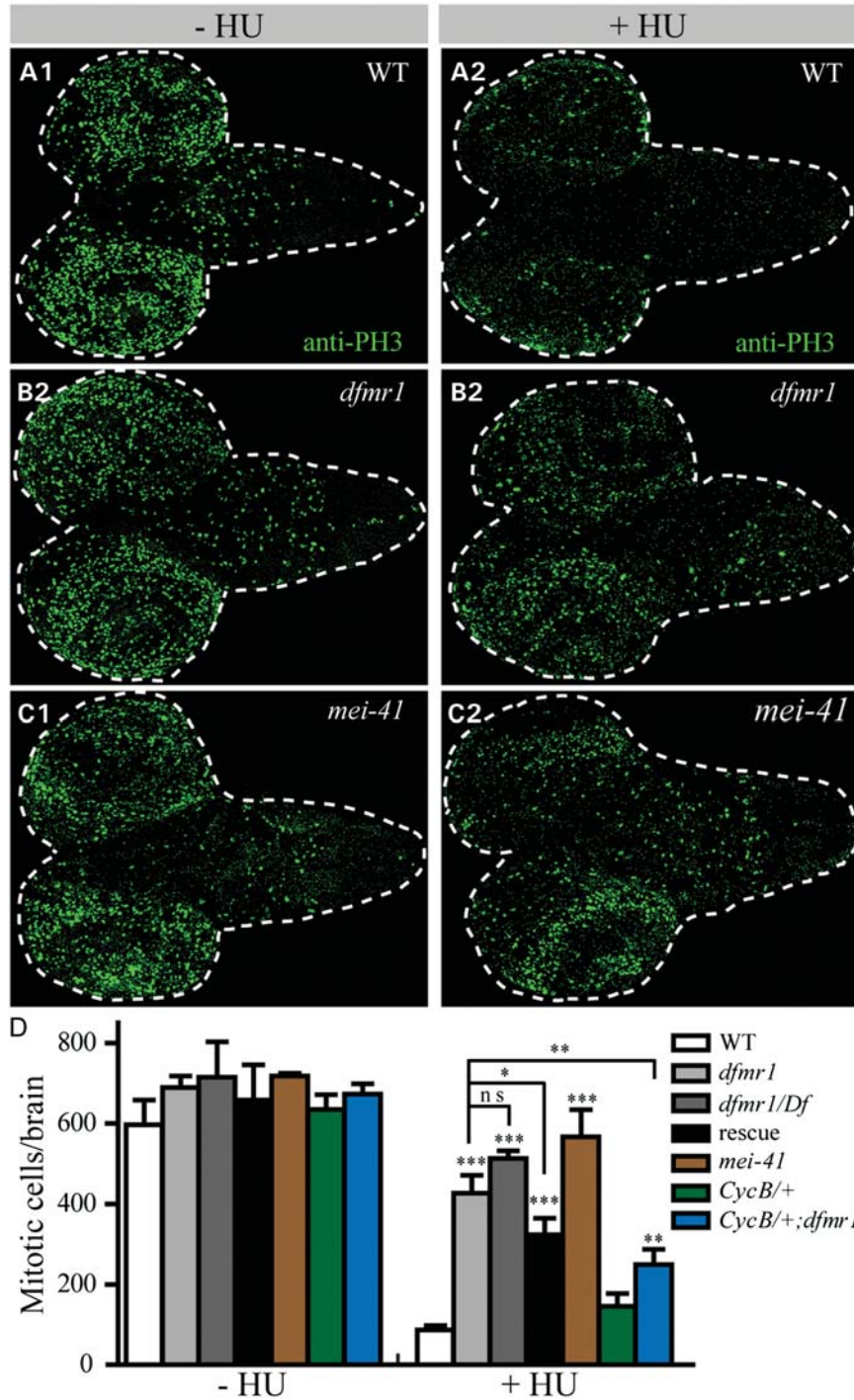


Figure 2. Defective G2/M checkpoint in the larval brains of *dfmr1* mutants. Brains from third-instar larvae mock-treated and treated with 50 mg/ml HU were stained with anti-PH3 antibody to detect mitotic cells. Wild-type (A), *dfmr1*^{50M} (B) and *mei-41*^{RT1} (C) mutants mock-treated (-HU; A1-C1) and HU-treated (A2-C2) were examined. There was a significant reduction in mitosis induced by HU in wild-type brains (A1 and A2), indicating an intact G2/M checkpoint activated by DNA damage. (D) Quantitative analysis of mitotic cells in different genotypes under different conditions. After HU treatment, mitosis was almost completely blocked in wild-type brains, while *mei-41*^{RT1} mutants exhibited a strong G2/M checkpoint defect as evidenced by virtually no decrease in the number of mitotic cells (brown bars). *dfmr1*^{50M} null mutants showed significantly more mitotic cells than the wild-type, while reducing the dose of *CycB* by half partially rescued the G2/M checkpoint defect in *dfmr1*^{50M} mutants. *n* ≥ 6; **P* < 0.05, ***P* < 0.01 and ****P* < 0.001; error bars indicate SEM.

dfmr1 mutants (Fig. 5B). In contrast to the increased levels of *CycB*, the other two mitotic cyclins *CycA* and *CycB3* (23,24) showed normal expression levels in *dfmr1* mutants with or

without HU treatment (Fig. 5A). These results together show that dFMRP specifically regulates the expression level of *CycB*.

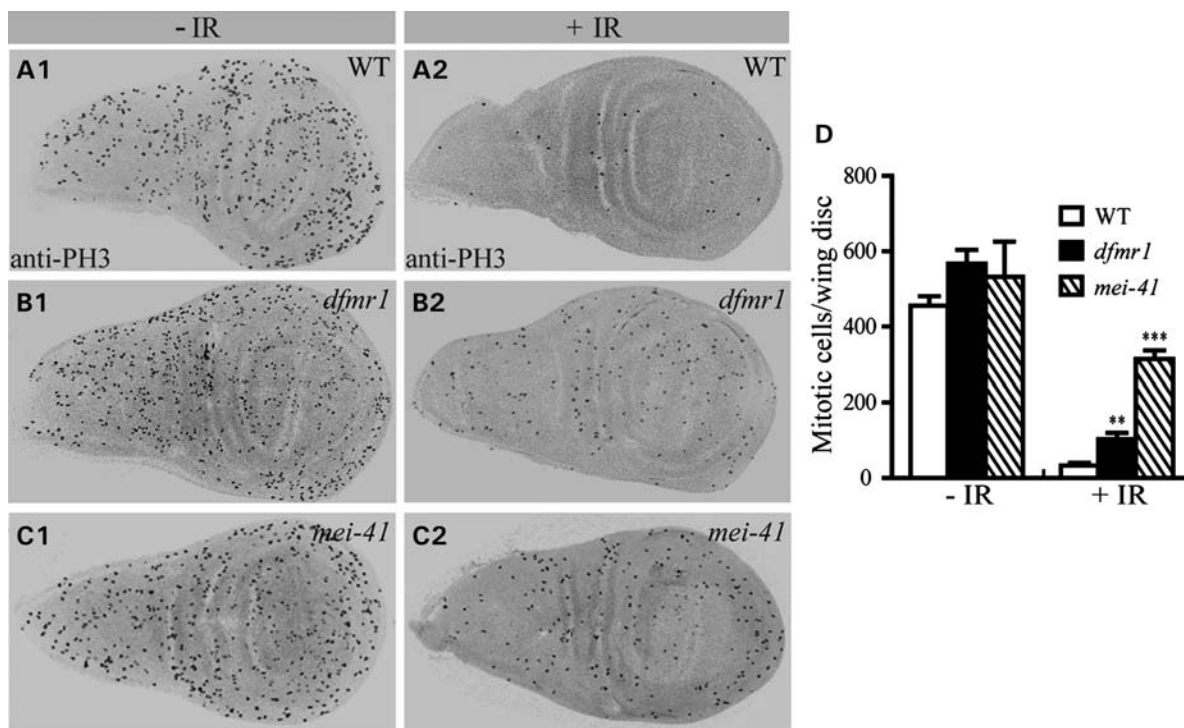


Figure 3. Defective G2/M checkpoint in the wing discs of *dfmr1* mutants in response to γ -ray radiation. Third-instar larvae were exposed to γ -irradiation at 40 Gy and wing discs were stained with anti-PH3 antibody to detect mitotic cells after 1 h recovery. Wild-type (A), *dfmr1*^{50M} (B) and *mei-41*^{RTI} (C) mutants were examined. Anti-PH3 staining results of the wing discs are shown for untreated (A1–C1) and IR-treated animals (A2–C2). (D) Quantitative analysis of mitotic cells in (A)–(C). Mitosis in the wing discs was almost completely blocked in IR-treated wild type, while *dfmr1*^{50M} mutants showed a mild increase in the number of mitotic cells compared with the *mei-41*^{RTI} mutants. $n \geq 5$ for each genotype; ** $P < 0.01$ and *** $P < 0.001$; error bars indicate SEM.

As the RNA-binding protein FMRP regulates the expression of multiple target genes at the post-transcriptional level, we performed RNA–protein immunoprecipitation to test whether *CycB* mRNAs were present in the dFMRP–RNA complexes. Background levels of *actin* mRNA served as a control (Fig. 5C). Indeed, the dFMRP-containing protein complex immunoprecipitated by anti-dFMRP from larval brains contained 6.3-fold more *CycB* mRNA transcripts than the *actin* transcripts (Fig. 5C), though the mRNA level of *CycB* in *dfmr1*^{50M} brain lysates was comparable with the wild-type (Supplementary Material, Fig. S2). The mRNA level of *futsch*, a known target of dFMRP (25), was also enriched by ~ 7.3 -fold compared with the *actin* controls (Fig. 5C). The enrichment of *CycB* mRNA transcripts in the dFMRP-containing complexes and the elevated expression of *CycB* protein in *dfmr1* mutants suggest that dFMRP may directly repress the translation of *CycB* mRNA.

Reducing *CycB* partially rescues the G2/M checkpoint defect and reverses the hypersensitivity to irradiation in *dfmr1* mutants

Elevated expression of *CycB* might be responsible for the G2/M checkpoint defect in *dfmr1* mutants. If so, then reducing the dosage of *CycB* could rescue the phenotypes of *dfmr1* mutants, including the G2/M checkpoint defect and the hypersensitivity to genotoxic agents. Indeed, a heterozygous *CycB* null mutation (*CycB*^{2/+}) significantly reduced the number of mitotic

cells in the *dfmr1*^{50M} brain after HU treatment (426.9 ± 44.8 for *dfmr1*^{50M} mutants and 249.5 ± 37.7 for *dfmr1*^{50M} mutants heterozygous for *CycB*²; $P < 0.01$; Fig. 2D). This indicates that the G2/M checkpoint defect that causes increased mitosis following DNA damage in *dfmr1* mutants is caused by the up-regulation of *CycB* expression. In addition, reducing the dose of *CycB* by half significantly increased the viability of *dfmr1*^{50M} mutants exposed to 30 Gy γ -ray radiation ($33.1 \pm 3.2\%$ survival) compared with the *dfmr1*^{50M} mutants alone ($14.2 \pm 4.4\%$ survival; $P < 0.01$; Fig. 5D). Thus, elevated *CycB* expression is at least partially responsible for the G2/M checkpoint defect and the hypersensitivity to irradiation in *dfmr1* mutants.

Ionizing radiation induces excessive p53-dependent apoptosis in *dfmr1* mutants

Cells with un-repaired DNA damage are eliminated by programmed cell death to avoid the proliferation of genetically mutated cells. Since *dfmr1* mutants exhibited hypersensitivity to DNA damage and a defective G2/M DNA damage checkpoint, we investigated whether apoptosis was normally induced in *dfmr1* mutants after irradiation using anti-caspase-3 staining. Spontaneous apoptosis was rarely observed in the wing discs of untreated flies (Fig. 6A1–D1), but substantial apoptosis was induced 4 h after irradiation in both wild-types and *dfmr1*^{50M} mutants (Fig. 6A2 and B2). Compared with wild-type, the caspase-3 index, defined as

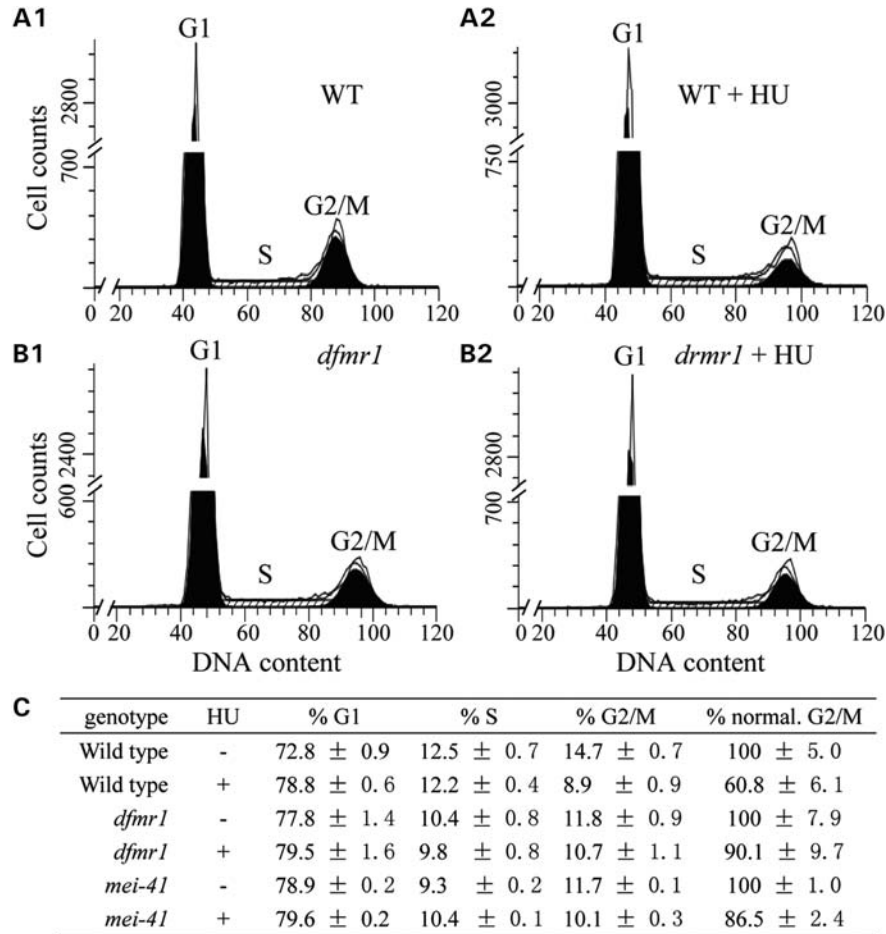


Figure 4. Altered profile of cell cycle phases in *dfmr1* mutants following HU treatment. (A and B) Flow cytometric analysis of larval brain cells from wild-type (A1–2) and *dfmr1*^{50M} mutant larvae (B1 and B2) with or without HU treatment. (C) Quantitative analysis of cell cycle phase distribution of wild-type, *dfmr1*^{50M} and *mei-41*^{RT1} mutants from multiple, independent samples. The fraction of cells in G2 and mitotic phases in *dfmr1* mutants after HU treatment was not obviously decreased compared with wild-type, suggesting a defective G2/M checkpoint in *dfmr1* mutants. For each sample, at least 10 000 cells were analyzed ($n = 3$).

the anti-caspase-3-positive area divided by the total wing disc area, was significantly increased in irradiated *dfmr1* mutants (0.13 ± 0.01 for *fmr1*^{50M} mutants versus 0.07 ± 0.008 for wild-type, $n \geq 8$; $P < 0.01$; Fig. 6E). One copy of the wild-type genomic *dfmr1* transgene fully rescued the increased apoptosis in *dfmr1* mutants (Fig. 6E), indicating that the excessive apoptosis after irradiation is specifically caused by loss of *dfmr1*.

It is well established that p53 is responsible for the irradiation-induced apoptosis in both *Drosophila* and mammals (26,27). We therefore tested whether the excessive apoptosis in irradiated *dfmr1*^{50M} mutants was p53-dependent. Irradiation-induced apoptosis was reduced to undetectable levels in both *p53*^{5A-1-4} null mutants and *dfmr1 p53* double null mutants (Fig. 6C2, D2 and E), indicating that the excessive apoptosis in *dfmr1* mutants following irradiation depends on p53.

Irradiation-induced p53-dependent apoptosis is mediated through the Reaper (Rpr)-Hid-Grim (RHG) pro-apoptotic proteins that are transcriptionally regulated by p53 (28,29). To provide further evidence for the excessive p53-dependent

apoptosis in irradiated *dfmr1* mutants, we quantified the level of RHG gene transcripts by quantitative PCR. Compared with the wild-type, the levels of *rpr*, *hid* and *grim* transcripts in irradiated *dfmr1*^{50M} mutant brains were significantly increased by 4.26-, 6.43- and 5.88-fold, respectively (Fig. 6F), indicating that increased apoptosis in *dfmr1* mutant is mediated through the RHG pro-apoptotic proteins.

We further analyzed the expression of *rpr* by examining the β -galactosidase activity of an *rpr-11-lacZ* reporter in the wing discs. The *rpr-11-lacZ* reporter, consisting of an irradiation-responsive *cis*-element and the p53-binding site of *rpr* fused to *lacZ*, has been used to assess the p53-mediated expression of *rpr* by irradiation (30,31). In the un-irradiated animals, the basal level of β -galactosidase expression occurred at the posterior wing margin and dorsal hinge of both wild-types and *dfmr1*^{50M} mutants (Fig. 6G1 and H1). After irradiation, an obviously higher level of β -galactosidase expression at the dorsal hinge and throughout the wing pouch was detected in *dfmr1* mutants compared with the wild-type (compare Fig. 6G2 and H2). Statistically, the percentage of the total area of the

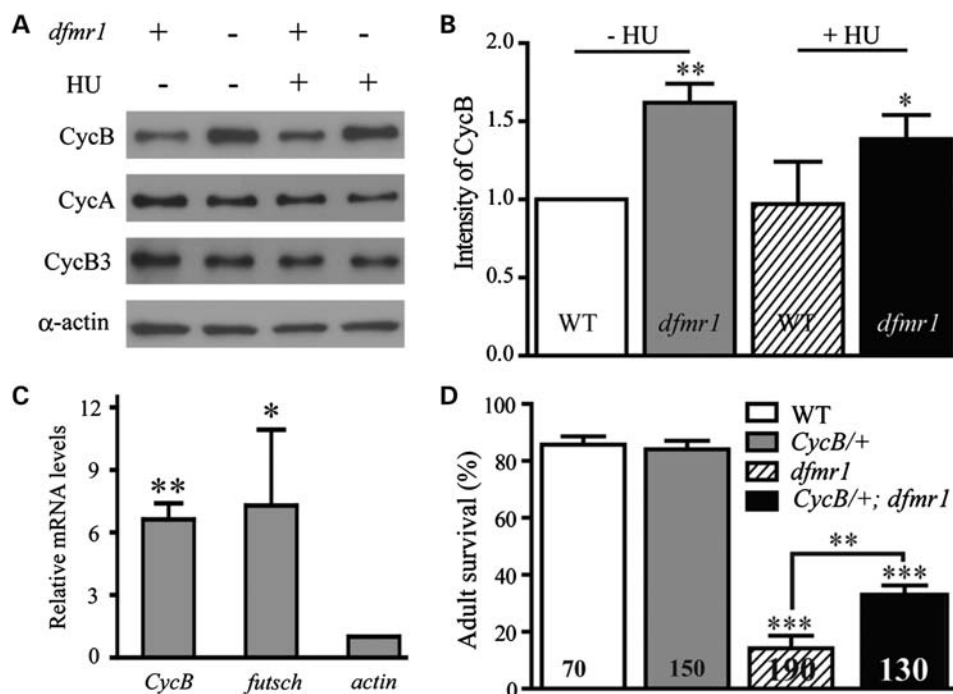


Figure 5. Suppression of CycB protein expression by dFMRP. (A) Expression of different cyclins was detected by western blotting of brain lysates from mock-treated and HU-treated wild-type and *dfmr1*^{50M} mutants. α -Actin was used as a loading control. (B) Densitometric quantification of western blotting results in (A). CycB protein expression in the larval brains was significantly higher in *dfmr1*^{50M} mutants than in the wild-type both un-treated ($n \geq 3$; $P < 0.01$) and after 50 mg/ml HU treatment ($n \geq 3$; $P < 0.05$), indicating that dFMRP normally acts to suppress CycB expression. No significant change in the expression levels of CycA and CycB3 was detected in different genotypes under different conditions. (C) *CycB* mRNA was significantly enriched in the dFMRP-containing protein complex ($n \geq 3$; $P < 0.01$). The mRNA levels of three different genes in the dFMRP immunoprecipitates from the larval brains of wild-types and *dfmr1*^{50M} mutants were determined by quantitative PCR. The mRNA levels are displayed as ratios (wild-type/mutant) of *CycB* and *futsch* normalized to the *actin* control in the immunoprecipitates. (D) Adult viability of different genotypes after irradiation of larvae at 30 Gy. *CycB*^{2/+} animals were as resistant to irradiation as wild-types. Reducing the dose of *CycB* by half partially rescued the radiation hypersensitivity of *dfmr1*^{50M} mutants. The number of animals tested are indicated; * $P < 0.05$, ** $P < 0.01$ and *** $P < 0.001$; error bars indicate SEM.

LacZ-positive signals per wing disc was $10.6 \pm 0.7\%$ in wild-types, but significantly increased to $16.9 \pm 1.8\%$ in *dfmr1*^{50M} mutants after irradiation ($n \geq 7$; $P < 0.01$). These results together demonstrate that the p53-mediated pathway is responsible for the excessive apoptosis in *dfmr1* mutants.

Increased number of DNA breaks in the irradiated *dfmr1* mutants

As *dfmr1* mutants displayed increased sensitivity to genotoxic stress (Fig. 1 and Table 1), we examined the expression of phosphorylated H2Av in the salivary gland cells following irradiation. Phosphorylation at serine 137 of the histone variant H2Av, the homolog of mammalian histone variant H2AX (32,33), is one of the early markers for DSBs. The number of phosphorylated H2Av foci per cell in the wing discs of un-treated *dfmr1*^{50M} mutants (0.25 ± 0.08 , $n = 292$ cells) was not significantly different from the wild-type controls (0.28 ± 0.05 , $n = 193$ cells; $P > 0.05$; Fig. 7C). One hour after irradiation at 40 Gy, however, the number of phosphorylated H2Av foci per cell was significantly higher in *dfmr1*^{50M} mutants (10.33 ± 0.83 , $n = 157$; Fig. 7B1–B3 and C) than the wild-type (6.76 ± 0.27 , $n = 113$; $P < 0.05$; Fig. 7A1–A3 and C). In addition, we found more chromosomal breaks in *dfmr1*

larval brain neuroblasts (0.71 ± 0.08 chromosomal breaks/nucleus, $n = 123$) compared with wild-types (0.38 ± 0.04 , $n = 86$; $P < 0.01$; Fig. 7D–F) after radiation. Moreover, reducing the dosage of *CycB* by half significantly reduced the number of chromosomal breaks in *dfmr1* mutants to the wild-type level (0.50 ± 0.04 , $n = 104$), suggesting that the phenotype is caused by the up-regulation of CycB. The increased number of DNA breaks in *dfmr1* mutants (Fig. 7A–F) indicate a DNA repair defect which may underlie the mutants' hypersensitivity to irradiation.

As the nucleolus is a DNA damage sensor (34), we detected nucleoli with an antibody against fibrillar. Fibrillar is an rRNA 2'-O-methyltransferase, a component of the small nuclear ribonucleoprotein particle (35). Immunostaining for fibrillar revealed that the nucleoli of the salivary gland cells from *dfmr1* mutants appeared fragmented; the number of nucleoli per cell in *dfmr1* mutants (1.87 ± 0.07 nucleoli/cell, $n = 131$) was significantly increased compared with wild-type (1.19 ± 0.03 nucleoli/cell, $n = 170$; $P < 0.01$; Fig. 7G–I). Following irradiation at 1 Gy, the nucleoli of both wild-type and *dfmr1* mutants were dramatically disrupted and even completely eliminated (data not shown). The increased number of DNA breaks following irradiation and the fragmented nucleoli in *dfmr1* mutants support that dFMRP is involved in the DNA damage response.

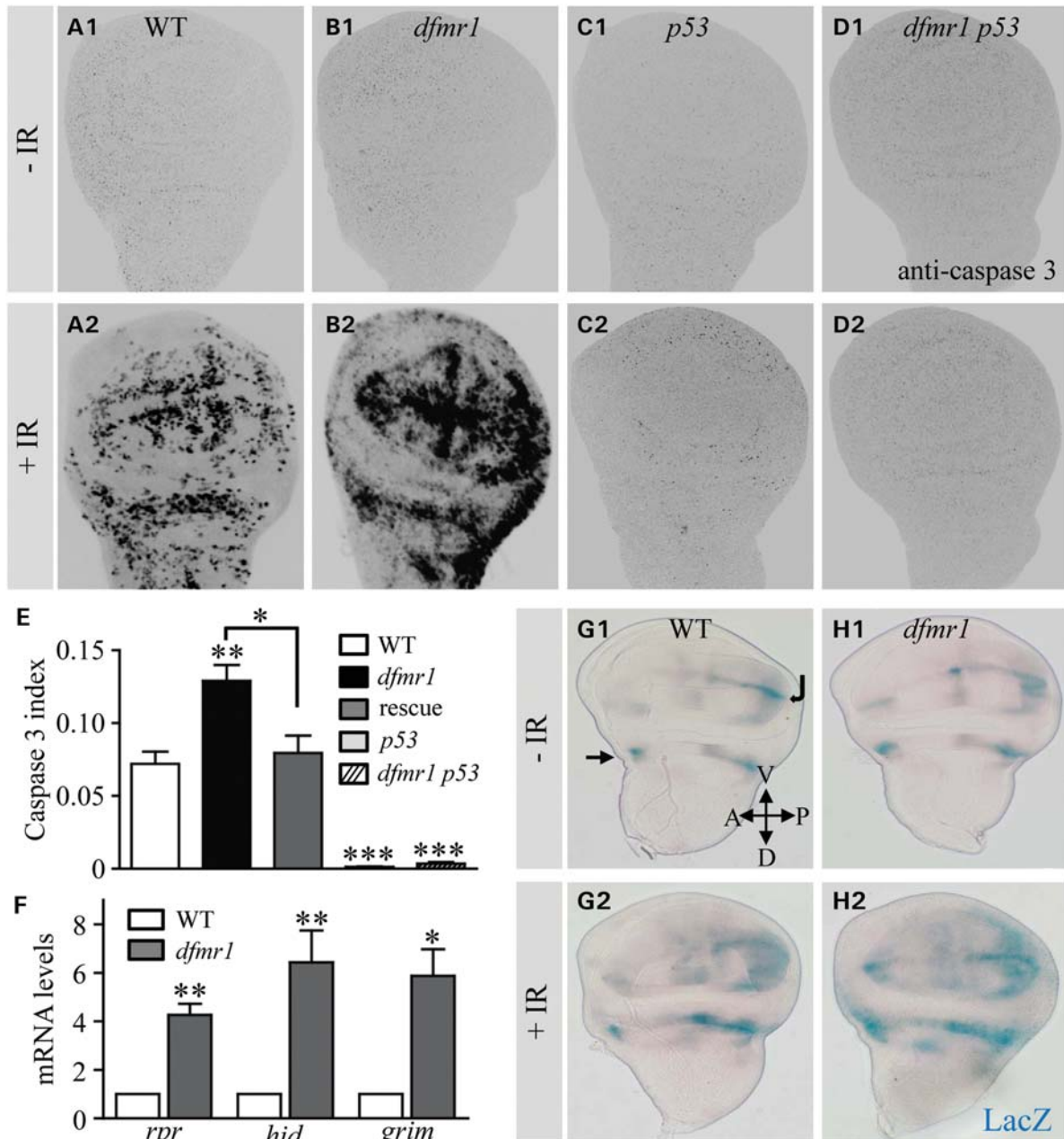


Figure 6. Increased p53-mediated apoptosis in *dfmr1* mutants in response to irradiation. Apoptosis detected by anti-caspase-3 staining in wing discs of wild-type (A), *dfmr1*^{50M} mutants (B), *p53*^{5A-1-4} mutants (C) and *dfmr1*^{50M} *p53*^{5A-1-4} double mutants (D). Staining results of untreated wing discs are shown in the top row (A1–D1), while samples prepared 4 h after 40 Gy radiation are presented in the bottom row (A2–D2). Spontaneous apoptotic cells were rare in all four genotypes, while significant numbers of apoptotic cells were induced by irradiation in both wild-type and *dfmr1*^{50M} mutants. (E) Apoptosis was quantified using anti-caspase-3 index, defined as the anti-caspase-3-positive area divided by the whole disc area, as an indicator. At least eight discs from three independent experiments were analyzed for each genotype. (F) Relative levels of *rpr*, *hid* and *grim* RNA normalized to the level of *rp49* transcripts were determined by quantitative PCR. $n \geq 3$ for each genotype; * $P < 0.05$ and ** $P < 0.01$; error bars indicate SEM. (G and H) Expression of β -galactosidase reflecting activation of the pro-apoptotic gene *rpr* was examined in wing discs. The level of β -galactosidase expression was similar in mock-treated wild-type and *dfmr1*^{50M} mutants (G1 and H1), but the β -galactosidase expression was higher in irradiated *dfmr1*^{50M} mutants compared with irradiated wild-types (G2 and H2). Arrow in G1 indicates the dorsal hinge and curved arrow points at the posterior wing margin.

dfmr1 mutants exhibit increased genome instability induced by genotoxic stress

As *dfmr1* mutants were hypersensitive to genotoxic stress, we carried out a loss-of-heterozygosity (LOH) assay in the adult wing hair system to assess genome instability caused

by irradiation (28,36). In the wild-type, a single hair is formed per hair cell in the adult wings (Fig. 8A), whereas in the homozygous nulls of the recessive *multiple wing hairs* (*mwh*¹), multiple hairs (ranging from 2 to 7) are formed by each hair cell (Fig. 8B). Whenever a precursor hair cell heterozygous for *mwh*¹ loses the wild-type copy

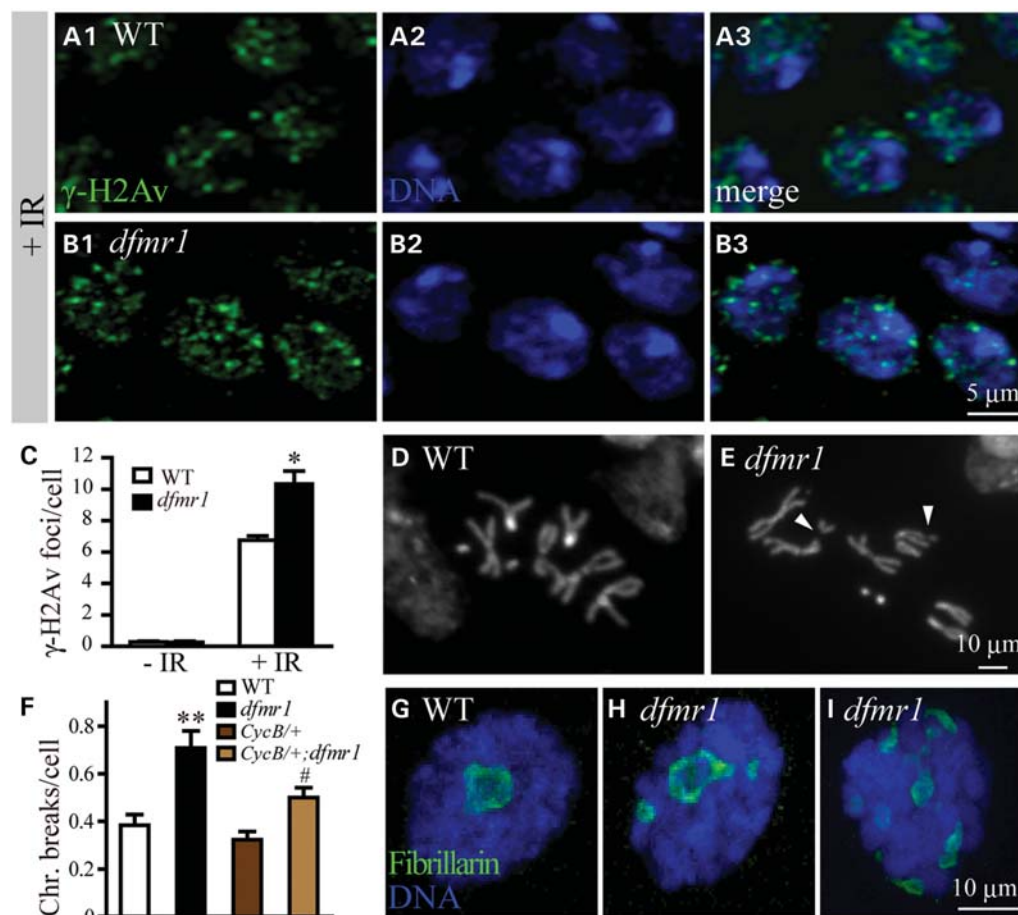


Figure 7. More irradiation-induced DNA breaks in *dfmr1* mutants. Wing discs from different genotypes were stained with anti-phosphorylated H2Av (γ -H2Av) (green) to detect DSBs and TO-PRO-3 iodide (blue) to detect nuclear DNA. There were more γ -H2Av foci in the nucleus of *dfmr1*^{50M} mutants (B1–B3) than those in wild-types (A1–A3) at 1 h after 40 Gy irradiation. (C) Quantitative results of the number of γ -H2Av foci per cell in the untreated (–IR) and irradiated (+IR) wing discs. $n \geq 113$ cells for each genotype; * $P < 0.05$; error bars indicate SEM. Representative metaphase chromosomes of larval neuroblasts from wild type (D) and *dfmr1*^{50M} mutants (E) 1 h after 10 Gy irradiation. Chromosomal breaks were indicated by arrowheads in (E). (F) The number of chromosomal breaks per nucleus in different genotypes. $n \geq 86$; ** $P < 0.01$ compared with wild-type, whereas # $P < 0.05$ compared with the mutants; error bars indicate SEM. The nucleolar organization in larval salivary gland cells detected with anti-Fibrillarin. Most cells in wild-type had one nucleolus (G), whereas most *dfmr1*^{50M} mutant cells had fragmented, multiple nucleoli (H and I).

(i.e. LOH) during proliferation, the progeny hair cells will show the *mwh* phenotype (Fig. 8C). Two *dfmr1* null alleles, *dfmr1*^{50M} and *dfmr1*³, were examined in the LOH assay. The number of *mwh* hair cells per wing in heterozygous *mwh*¹ animals in the wild-type background (1.0 ± 0.75) was similar to that in the *dfmr1* null background (0.5 ± 0.5 for *dfmr1*^{50M} and 0.7 ± 0.3 for *dfmr1*³; $P > 0.05$ for both *dfmr1* alleles compared with the wild-type; Fig. 8D). After irradiation at 20 Gy, however, both *dfmr1* null lines heterozygous for *mwh*¹ exhibited a significantly larger number of multiple hair cells per wing (73.4 ± 3.0 for *dfmr1*^{50M} and 64.0 ± 3.5 for *dfmr1*³) compared with the irradiated wild-type controls (30.6 ± 1.4 ; $P < 0.001$ for both alleles; Fig. 8D). The increased incidence of the multiple wing hair phenotype suggests that the single wild-type copy of the *mwh* gene is more often lost or disrupted in *dfmr1* mutants than in the wild-types after irradiation. Thus, our data show that, in the context of genotoxic stress, dFMRP is required for maintaining genome stability.

DISCUSSION

Loss of *dfmr1* leads to hypersensitivity to genotoxic stress and defective G2/M DNA damage checkpoint

Phenotypic analysis of animal models of FXS continues to reveal novel functions for FMRP. In this study, we present multiple lines of experimental evidence demonstrating for the first time that dFMRP is involved in DNA damage response. DNA damage responses are executed through coordinated interplays and cross-talks of multiple players from sensors to transducers, and finally to effectors. There are four distinct pathways involved in the DNA damage response: cell cycle arrest (also known as DNA damage checkpoint), transcriptional induction, DNA repair and apoptosis; the four pathways act independently under certain conditions, but frequently, they interact to repair the damaged DNA or commit apoptosis (8,13,18,37). The hypersensitivity to irradiation (Fig. 1), G2/M checkpoint defects (Figs 2–4), excessive apoptosis (Fig. 6) and increased number of DNA breaks (Fig. 7) in

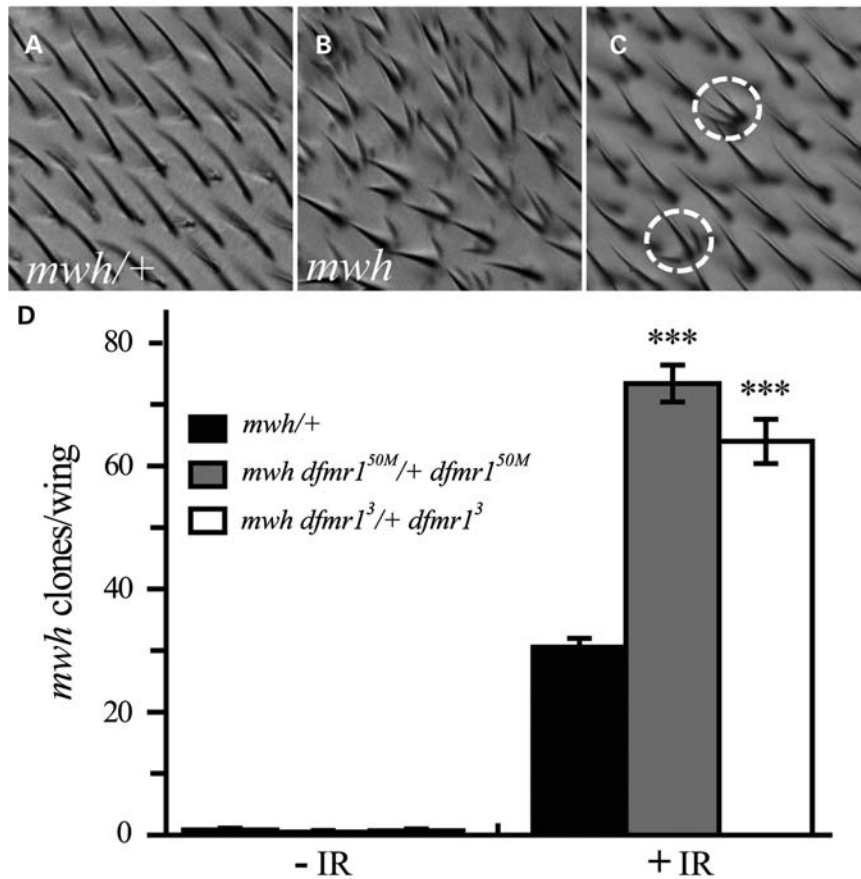


Figure 8. Increased genome instability in *dfmr1* mutants upon irradiation revealed by the LOH assay. (A) Micrograph showing one hair per adult wing cell in *mwh*¹ heterozygous mutants. (B) Two or more hairs per cell in homozygous *mwh*¹ mutants. (C) Multiple hairs per cell (round circles) in adult flies heterozygous for *mwh*¹ in the *dfmr1*^{50M} null background following 20 Gy radiation of third-instar larvae. Cells in circles lost the only wild-type copy of *mwh* due to genome instability. (D) The number of *mwh*¹ clones per wing in wild-type and *dfmr1*^{50M} mutants. In the absence of irradiation, the frequency of spontaneous *mwh*¹ clones per wing was low and indistinguishable between *dfmr1* mutants and wild-types. However, there were significantly more *mwh*¹ clones per wing in *dfmr1*^{50M} mutants compared with the wild-type following irradiation. Two *dfmr1* null alleles *dfmr1*^{50M} and *dfmr1*³ were analyzed. $n \geq 6$ for each genotype. *** $P < 0.001$; error bars indicate SEM.

dfmr1 mutants after irradiation all support that *dfmr1* plays a critical role in DNA damage response.

In addition, *dfmr1* mutants showed an elevated rate of LOH upon DNA damage (Fig. 8), indicating reduced genome stability in *dfmr1* mutants. It is well established that proteins involved in checkpoint control and DNA repair play a critical role in maintaining genome integrity (9,38). Thus, the decreased genome stability in *dfmr1* mutants also supports the conclusion that *dfmr1* participates in DNA damage response.

Loss of *dfmr1* affects cell cycle progression in different developmental processes (4,5,7). We speculated that the hypersensitivity to DNA damage in *dfmr1* mutants might be due to a defective cell cycle control. However, in the absence of genotoxic stress, we detected normal expression of the G1/S checkpoint regulator CycE (data not shown), normal DNA synthesis activity (Supplementary Material, Fig. S1) and normal G2/M checkpoint (Figs 2 and 3) in *dfmr1*^{50M} mutants compared with the wild-type. These results indicate that the G1/S and G2/M checkpoints were functional in *dfmr1* mutants. Following genotoxic stress, however, we found significantly more mitotic cells

in the larval brains and wing discs of *dfmr1*^{50M} mutants compared with the wild-type controls (Figs 2 and 3), indicating a defect in the G2/M DNA damage checkpoint in *dfmr1* mutants. In support of this checkpoint defect, cell cycle profiling of the larval brain cells by flow cytometry demonstrated a similar trend of cell cycle profile between *dfmr1* and *mei-41* mutants (Fig. 4). We therefore conclude that *dfmr1* primarily regulates the G2/M checkpoint in response to genotoxic stress.

The defective G2/M checkpoint in *dfmr1* mutants under genotoxic stress is caused by up-regulation of CycB

Cyclins and their CDK partners play an important role in regulating cell cycle progression. Misregulation of these cyclin-CDK complexes causes defective cell cycle progression, especially in the cells with damaged DNA (21,39). When DNA damage is inflicted at the G1 stage, the G1/S checkpoint regulator CycE-CDK2 is silenced to arrest the G1 to S transition. Alternatively, when DNA damage occurs at the G2 stage or if DNA damage remains unrepaired from the previous G1 or S phase, the CycB-CDK1 complex (also known as a mitosis

promoting factor) is inhibited to arrest cells at the G2/M transition (21,22). In light of a report demonstrating that dFMRP suppresses the expression of *CycB* at the mid-blastula transition during early embryonic development (4), we speculated that the G2/M checkpoint defect observed in *dfmr1* mutants after genotoxic stress might be due to the altered expression of *CycB*. Indeed, *CycB* protein was elevated in *dfmr1*^{50M} brains, while the other two G2/M checkpoint regulators, *CycA* and *CycB3*, were unaltered (Fig. 5), indicating a specific suppression of *CycB* by dFMRP. This specific regulation of *CycB* by dFMRP was further supported by the observation that *CycB* mRNA was enriched in the dFMRP-mRNA protein complex from larval brains (Fig. 5). Moreover, reducing the dose of *CycB* by half partially rescued the increased mitosis and hypersensitivity of *dfmr1* mutants to genotoxic stress (Figs 2 and 5). Thus, up-regulation of *CycB* in *dfmr1* mutants accounts, at least partially, for the G2/M checkpoint defect in response to DNA damage. In support of this conclusion, overexpression of the truncated, stable form of *CycB* is sufficient to induce G2/M transition defect in both eye discs and wing discs after irradiation (Supplementary Material, Fig. S3, but also see Supplementary Material, Fig. S4).

The *CycB* level is tightly regulated during the cell cycle at both the transcriptional and post-translational levels. Among the many regulators of *CycB*, the transcription factors NF-Y, FoxM1 and B-Myb activate transcription of *CycB* (22,40). These *CycB* regulators are important for the G2/M progression under both normal and stress conditions. Activation of FoxM1 is critical for the G2/M arrest (41,42), whereas B-Myb is required for the recovery of G2/M checkpoint in p53-negative cells (43). In this study, we reveal a negative regulation of *CycB* by dFMRP at the post-transcriptional level that controls the G2/M checkpoint under genotoxic stress.

***dfmr1* inhibits DNA damage-induced apoptosis and preserves genome integrity**

In addition to the G2/M cell cycle defect in *dfmr1* mutants (Figs 2–5), we found an obviously disrupted nucleolar structure in the mutant salivary gland cells (Fig. 7). As the nucleolus is critical for the DNA damage-induced p53 activation and apoptosis (34,44), we examined apoptosis in the wing discs by anti-caspase-3 staining. Spontaneous apoptosis was undetectable in the untreated *dfmr1* mutants and wild-types, while genotoxic stress evoked excessive p53-dependent apoptosis in *dfmr1* mutants (Fig. 6). Overactivation of p53 in the *dfmr1* mutants was further confirmed by elevated expressions of the pro-apoptotic *hid-rpr-grim* genes transcriptionally regulated by p53 (Fig. 6F–H). It is unknown at present why *dfmr1* mutants showed increased p53-dependent apoptosis after irradiation. One interpretation for the phenotype is compromised DNA damage repair in *dfmr1* mutants (Fig. 7). Alternatively, the increased level of *CycB* in *dfmr1* mutants may also lead to elevated apoptosis (Fig. 5 and Supplementary Material, Fig. S3, but also see Supplementary Material, Fig. S4). It is worth noting that without genotoxic stress, *dfmr1* is required for apoptosis and clearance of developmentally transient neurons in the adult brains (45). On the other hand, overexpression of dFMRP in multiple tissues including the wings and eyes also induces apoptosis, though a possible

role of p53 in the process was not examined (46). Thus, dFMRP can either promote or inhibit apoptosis under different conditions by distinct yet uncharacterized mechanisms.

Drosophila dfmr1 null mutants also exhibited decreased genome stability as revealed by the LOH assay (Fig. 8). Apoptosis is an endogenous and well conserved program to eliminate cells with severely damaged DNA to avoid propagation of potential mutations (47). It is conceivable that loss of *dfmr1* decreases genome stability, presumably resulting from a DNA repair defect, leading to increased apoptosis and lethality following DNA damage. Further experiments are required to unravel the causal relationships between dFMRP, DNA repair and apoptosis.

It is not known if FXS patients and *Fmr1* knockout mice are also hypersensitive to genotoxic stress. It is well established that the fragile sites of chromosomes are more prone to DNA damage and thus more dependent on the integrity of DNA repair mechanisms to maintain chromosomal stability (48,49). A recent study using fibroblasts reported that the DNA damage response is required to maintain the stability of the fragile X site (50). In addition, mutagen-induced genome instability was observed in the cultured lymphocytes from FXS patients (51,52). However, a subsequent study reported that lymphocytes from FXS patients displayed normal genome stability under genotoxic stress (53). This discrepancy remains to be resolved. In *Drosophila*, there is only one FMRP homolog instead of three FMRP family members in mammals (14,46). The redundancy of three FMRP members in mammals may make the phenotype of single mutants too weak to be detected. It would be of interest to test if double or triple mouse knockouts of the three FMRP family members exhibit the hypersensitivity to genotoxic stress observed in the *Drosophila dfmr1* mutants. Such a result would underscore a novel role for FMRP in maintaining genome stability and cell cycle control to allow for proper neuronal proliferation during brain development.

MATERIALS AND METHODS

***Drosophila* stocks and genetics**

All fly stocks were cultured at 25°C on standard cornmeal medium unless specified. The *w*¹¹¹⁸ was used as the wild-type strain. Two independently *dfmr1* null alleles, *dfmr1*^{50M} and *dfmr1*³, were described previously (25,54). A wild-type genomic *dfmr1* transgene strain *P[w+ : dfmr1]* was a generous gift from Dr H. Siomi (16). The *rpr-11-LacZ/CyO GFP* reporter was from Dr J.M. Abrams (55). The stocks *cycB*², *mwh*¹, *mei-41*^{RT1}, *p53*^{5A-1-4} and *Df(3R)BSC38* uncovering *dfmr1* were obtained from the Bloomington *Drosophila* Stock Center (Bloomington, IN, USA). The *dfmr1 p53* and *mwh dfmr1* double mutants were generated by conventional genetic techniques.

Ionizing radiation assay

For the radiation sensitivity test, *Drosophila* larvae were irradiated as described previously (28). Specifically, wandering third-instar larvae in glass vials were irradiated at the intensity of ~1 Gy/min for a serial of doses of 0, 5, 10, 20, 30 and 40 Gy in a ⁶⁰Co irradiator (Department of Applied Chemistry,

Peking University). One week following irradiation, the number of surviving adults was scored. The percentage of surviving adults of a specific genotype to the total number of larvae irradiated is presented. Each treatment was repeated three times and at least 60 larvae were assayed for each dose (Fig. 1).

MMS and HU sensitivity assay

The mutagen sensitivity assay was conducted as described previously (17). Briefly, 20 *dfmr1*^{50M}/*TM6B* *Tb* *Hu* females were mated with several males for 24 h to allow egg laying and then transferred to new vials. Fifty microliters of MMS (Sigma) or HU (Sigma) at different concentrations was added to vials containing larvae at 24–48 h after egg laying, and ddH₂O was used as a mock control. Adult flies were scored within 2 weeks of the mutagen treatment, and the percentage of *dfmr1*^{50M} homozygotes to the total number of surviving adults was calculated. Each treatment was repeated three times and at least 144 total progeny were scored for each dose.

Immunohistochemistry

Different tissues from third-instar larvae were dissected in phosphate-buffered saline (PBS), fixed in 4% formaldehyde for 25 min, and blocked in blocking solution (1% bovine serum albumin and 2% goat serum in 0.3% PBST) for 30 min. For the examination of the G2/M checkpoint, third-instar larvae were fed 50 mg/ml of HU for 5 h following a published protocol (56) or irradiated at 40 Gy. Brains and ventral nerve cords and wing discs from third-instar larvae were stained with rabbit anti-PH3 (1:500; Millipore) to detect mitotic cells.

For detecting DSBs, third-instar larvae were irradiated at 40 Gy and stained after 1 h recovery with a rabbit antibody against the phosphorylated *Drosophila* H2Av (also known as H2AvD; 1:200; Rockland). Mouse anti-fibrillarin (1:1000; Covance) was used for nucleolar staining. Nuclear DNA was detected by TO-PRO-3 iodide (1:2000; Invitrogen) staining. The secondary antibodies used were Alexa 488 or 568-conjugated anti-mouse or anti-rabbit antibodies (1:1000; Invitrogen). All immunostained samples were mounted with Vectashield (Vector Laboratories, Burlingame, CA, USA) and images were collected with a Leica SP5 confocal microscope and processed using Adobe Photoshop.

Flow cytometry

To examine the cell cycle profile of larval brain cells, wandering third-instar larvae were cultured in the food containing 50 mg/ml of HU for 5 h before dissection. Brains from 20 un-treated and 20 treated larvae were dissected out in PBS. After the removal of PBS, 600 μ l ice-cold buffer (200 mM Tris-HCl, pH 7.5, 4 mM MgCl₂, 0.1% Triton X-100) was added to the brains. The samples (three replicates) were then transferred to a Petri dish and chopped with a single-edged razor blade until homogenous. The samples were placed into flow cytometry tubes by filtration through a 40 μ m mesh (BD BioSciences). After adding Hoechst 33342 (10 μ g/ml), samples containing largely single cells were kept on ice for 1 h before analysis on

a BD FACS Aria II flow cytometer (BD BioSciences). Reading with coefficient of variation, values <6% were analyzed using ModFit (Verity Software House) software.

Western analysis

Forty brains from wandering third-instar larvae treated with 50 mg/ml of HU and mock-treated for 5 h were dissected in PBS and homogenized in 50 μ l lysis buffer [100 mM KCl, 2 mM MgCl₂, 50 mM Tris (pH 7.5), 2 mM ethylene glycol tetraacetic acid, 2% (v/v) glycerol, 0.125% (v/v) Triton X-100, 100 nM paclitaxel (Invitrogen), 1% (v/v) DMSO and 1% Protease Inhibitor Cocktail (Calbiochem)] followed by mixing with 5 \times loading buffer as described previously (57). Ten microliters of each sample was loaded on each gel lane. The primary antibodies used were anti-CycB3 [1:1000; from C.F. Lehner (24)], anti-CycB and anti-CycA (both used at 1:500; from the Developmental Studies Hybridoma Bank) and anti-actin (1:50 000; Millipore). The primary antibodies were detected by horseradish peroxidase-coupled secondary antibodies using a chemiluminescent method (ECL Kit, Amersham).

Quantification of mRNA transcripts

Immunoprecipitation of dFMRP-positive RNA-protein complex from wild-types and *dfmr1*^{50M} null mutants was performed as described previously (25,58). Briefly, ~200 third-instar larval brains were dissected out and homogenized in 1 ml ice-cold polysome lysis buffer (100 mM KCl, 5 mM MgCl₂, 10 mM hydroxyethyl piperazineethanesulfonic acid, pH 7.0, 0.5% Nonidet P-40, 1 mM dithiothreitol, 2 mM vanadylribonucleoside complexes solution) with 1 \times protease inhibitors (Calbiochem) and 100 U/ml RNase inhibitor RNasin (Promega). Brain lysate was incubated with a dFMRP antibody (6A15, Sigma) or mouse IgG at 4°C overnight. Fifty microliters of protein A-agarose beads (GE) was added and incubated for 4 h. After washing with polysome lysis buffer containing 1 M urea, the processed beads were resuspended in 100 μ l of polysome lysis buffer containing 0.1% SDS and 30 μ g proteinase K and incubated at 50°C for 30 min. RNA was extracted by conventional methods. The RNA was reverse transcribed with an oligo-dT primer using a kit from Invitrogen. *CycB* transcript was quantified with primers 5'-GGGAAACATCAGTTAGTTAAAACG-3' and 3'-CAGGTCACTGCCAGCAACTTAGGA-5' using a real-time PCR system Mx3000P (Stratagene) with a SYBR Green dye (Applied Biosystems). Primers for detecting *futsch* (available upon request) and *actin* mRNA were described previously (26,27). Statistical analysis was based on a minimum of three repeats.

For quantitative analysis of pro-apoptotic gene transcripts, total RNA was extracted from imaginal discs with Trizol reagent and reverse transcribed with an oligo-dT primer using a kit from Invitrogen. The transcript levels of *hid*, *rpr* and *grim* were quantified using a real-time PCR system Mx3000P (Stratagene) with a SYBR Green dye (Applied Biosystems) and normalized to the expression level of *rp49* as described previously (59). Three independent repeats were

performed for statistical analysis. Real-time PCR primer pairs were designed with Primer 3 software and tested by gel electrophoresis. The primer sequences were: rp49 F: TACAGGCCCAAGATCGTGAAG, rp49 R: GACGCACTCTGTTGTCGATACC; reaper F: CCAGTTGTGTAATTCCGAACGA, reaper R: TCGCCTGATCGGGTATGTAGA; hid F: AGGATGAGCGCGAGTACCAG, hid R: GCTGCTGCTCGAGTGGCTAT; grim F: CAATTCCTGCCAATATTCC, grim R: TCCTCATCGTTGTTCTGACC.

Analysis of apoptosis and chromosomal breaks

For apoptosis analysis, wing discs from third-instar larvae 4 h after irradiation at 40 Gy of different genotypes were dissected out in PBS and fixed in 4% formaldehyde at room temperature for 20 min. Samples were permeabilized in a buffer containing 100 mM sodium citrate and 0.1% Triton X-100 at 65°C for 30 min, incubated with rabbit anti-cleaved caspase-3 (1:200, Cell Signaling Technology) overnight at 4°C. Fluorescence-labeled secondary antibodies were used to detect the anti-caspase 3. Anti-caspase-3 index is defined as the ratio of the anti-caspase-3-positive area to the total disc area calculated using ImageJ.

Mitotic chromosomes of larval brains were performed essentially as described (60). Larvae were irradiated with 10 Gy γ -rays. After recovered at 25°C for 1 h, larval brains were dissected in PBS, incubated in a hypotonic solution (0.5% sodium citrate) for 10 min and fixed in a freshly prepared acetic acid/methanol/H₂O (11:11:2) mixture for a few seconds. Fixed brains were treated in 45% acetic acid for 1–2 min, followed by squashing. Chromosomes were stained with 4',6-diamidino-2-phenylindole in a mounting medium. Images were taken using a Zeiss ApoTome microimaging system.

LOH assay

The LOH assay was conducted as described previously (28,36). Wandering third-instar larvae of different genotypes were mock-treated or irradiated at a moderate dose of 20 Gy. Adult wings were dissected and dehydrated in isopropanol before mounting with glycerol. Five to ten wings were examined for each genotype using a Zeiss ApoTome microimaging system. Cells with more than one hair were scored as *mwh*¹ mutant cells.

Quantification and statistical analysis

To quantify the signal intensity in confocal images and western blots, ImageJ software was used. All statistical comparisons were performed using Microsoft Excel. *P*-values were calculated by two-tailed Student's *t*-tests. All data are presented as the mean \pm SEM. No asterisk denotes *P* > 0.05; asterisk denotes *P* < 0.05; double-asterisk denotes *P* < 0.01; triple-asterisk denotes *P* < 0.001.

SUPPLEMENTARY MATERIAL

Supplementary Material is available at *HMG* online.

ACKNOWLEDGEMENTS

We thank T. Jongens for *dfmr*¹³ mutants, H. Siomi for the wild-type genomic *dfmr* transgene *P*[*w+*:*dfmr*] line, J. Abrams for the *rpr-11-LacZ* reporter flies, C.F. Lehner for anti-CycB3, F. Zu for flow cytometry assay, Y. Wang for chromosomal break analysis and J. Wang for generating double mutants. We are grateful to the Bloomington Stock Centre for other fly stocks and the Developmental Studies Hybridoma Bank, University of Iowa for antibodies. γ -Ray radiation was carried out in the Department of Applied Chemistry, Peking University. We thank Y.S. Rong, R. Jiao, T.T. Su, D. Zarnescu and members of the Y.Q.Z. and X.B. laboratories for helpful discussions and critical comments on the manuscript.

Conflict of Interest statement. None declared.

FUNDING

This work was supported by the National Science Foundation of China (30930033 and 31110103907) to Y.Q.Z. and the National Basic Research Program of China (973 Program Grant No 2010CB934004) to X.B.

REFERENCES

1. Penagarikano, O., Mulle, J.G. and Warren, S.T. (2007) The pathophysiology of fragile x syndrome. *Annu. Rev. Genomics Hum. Genet.*, **8**, 109–129.
2. Castren, M., Tervonen, T., Karkkainen, V., Heinonen, S., Castren, E., Larsson, K., Bakker, C.E., Oostra, B.A. and Akerman, K. (2005) Altered differentiation of neural stem cells in fragile X syndrome. *Proc. Natl Acad. Sci. USA*, **102**, 17834–17839.
3. Luo, Y., Shan, G., Guo, W., Smrt, R.D., Johnson, E.B., Li, X., Pfeiffer, R.L., Szulwach, K.E., Duan, R., Barkho, B.Z. *et al.* (2010) Fragile x mental retardation protein regulates proliferation and differentiation of adult neural stem/progenitor cells. *PLoS Genet.*, **6**, e1000898.
4. Papoulas, O., Monzo, K.F., Cantin, G.T., Ruse, C., Yates, J.R. 3rd, Ryu, Y.H. and Sisson, J.C. (2010) dFMRP and Caprin, translational regulators of synaptic plasticity, control the cell cycle at the *Drosophila* mid-blastula transition. *Development*, **137**, 4201–4209.
5. Epstein, A.M., Bauer, C.R., Ho, A., Bosco, G. and Zarnescu, D.C. (2009) *Drosophila* fragile X protein controls cellular proliferation by regulating *cbl* levels in the ovary. *Dev. Biol.*, **330**, 83–92.
6. Yang, Y., Xu, S., Xia, L., Wang, J., Wen, S., Jin, P. and Chen, D. (2009) The bantam microRNA is associated with *Drosophila* fragile X mental retardation protein and regulates the fate of germline stem cells. *PLoS Genet.*, **5**, e1000444.
7. Callan, M.A., Cabernard, C., Heck, J., Luois, S., Doe, C.Q. and Zarnescu, D.C. (2010) Fragile X protein controls neural stem cell proliferation in the *Drosophila* brain. *Hum. Mol. Genet.*, **19**, 3068–3079.
8. Harper, J.W. and Elledge, S.J. (2007) The DNA damage response: ten years after. *Mol. Cell*, **28**, 739–745.
9. Lobrich, M. and Jeggo, P.A. (2007) The impact of a negligent G2/M checkpoint on genomic instability and cancer induction. *Nat. Rev. Cancer*, **7**, 861–869.
10. Maity, A., McKenna, W.G. and Muschel, R.J. (1995) Evidence for post-transcriptional regulation of cyclin B1 mRNA in the cell cycle and following irradiation in HeLa cells. *EMBO J.*, **14**, 603–609.
11. Maity, A., Hwang, A., Janss, A., Phillips, P., McKenna, W.G. and Muschel, R.J. (1996) Delayed cyclin B1 expression during the G2 arrest following DNA damage. *Oncogene*, **13**, 1647–1657.
12. Kao, G.D., McKenna, W.G., Maity, A., Blank, K. and Muschel, R.J. (1997) Cyclin B1 availability is a rate-limiting component of the radiation-induced G2 delay in HeLa cells. *Cancer Res.*, **57**, 753–758.
13. Song, Y.H. (2005) *Drosophila melanogaster*: a model for the study of DNA damage checkpoint response. *Mol. Cell*, **19**, 167–179.

14. Zhang, Y.Q. and Broadie, K. (2005) Fathoming fragile X in fruit flies. *Trends Genet.*, **21**, 37–45.
15. Callan, M.A. and Zarnescu, D.C. (2011) Heads-up: new roles for the fragile X mental retardation protein in neural stem and progenitor cells. *Genesis.*, **49**, 424–440.
16. Inoue, S., Shimoda, M., Nishinokubi, I., Siomi, M.C., Okamura, M., Nakamura, A., Kobayashi, S., Ishida, N. and Siomi, H. (2002) A role for the *Drosophila* fragile X-related gene in circadian output. *Curr Biol*, **12**, 1331–1335.
17. Abdu, U., Klovstad, M., Butin-Israeli, V., Bakhrat, A. and Schupbach, T. (2007) An essential role for *Drosophila* hus1 in somatic and meiotic DNA damage responses. *J Cell Sci*, **120**, 1042–1049.
18. Zhou, B.B. and Elledge, S.J. (2000) The DNA damage response: putting checkpoints in perspective. *Nature*, **408**, 433–439.
19. Laurencon, A., Purdy, A., Sekelsky, J., Hawley, R.S. and Su, T.T. (2003) Phenotypic analysis of separation-of-function alleles of MEI-41, *Drosophila* ATM/ATR. *Genetics*, **164**, 589–601.
20. Kondo, S. and Perrimon, N. (2011) A genome-wide RNAi screen identifies core components of the G-M DNA damage checkpoint. *Sci Signal*, **4**, rs1.
21. Kastan, M.B. and Bartek, J. (2004) Cell-cycle checkpoints and cancer. *Nature*, **432**, 316–323.
22. Lindqvist, A., Rodriguez-Bravo, V. and Medema, R.H. (2009) The decision to enter mitosis: feedback and redundancy in the mitotic entry network. *J Cell Biol*, **185**, 193–202.
23. Knoblich, J.A. and Lehner, C.F. (1993) Synergistic action of *Drosophila* cyclins A and B during the G2-M transition. *Embo J*, **12**, 65–74.
24. Jacobs, H.W., Knoblich, J.A. and Lehner, C.F. (1998) *Drosophila* Cyclin B3 is required for female fertility and is dispensable for mitosis like Cyclin B. *Genes Dev*, **12**, 3741–3751.
25. Zhang, Y.Q., Bailey, A.M., Matthies, H.J., Renden, R.B., Smith, M.A., Speese, S.D., Rubin, G.M. and Broadie, K. (2001) *Drosophila* fragile X-related gene regulates the MAP1B homolog Futsch to control synaptic structure and function. *Cell*, **107**, 591–603.
26. Ollmann, M., Young, L.M., Di Como, C.J., Karim, F., Belvin, M., Robertson, S., Whittaker, K., Demsky, M., Fisher, W.W., Buchman, A. et al. (2000) *Drosophila* p53 is a structural and functional homolog of the tumor suppressor p53. *Cell*, **101**, 91–101.
27. Wichmann, A., Jaklevic, B. and Su, T.T. (2006) Ionizing radiation induces caspase-dependent but Chk2- and p53-independent cell death in *Drosophila melanogaster*. *Proc. Natl Acad. Sci. USA*, **103**, 9952–9957.
28. Sogame, N., Kim, M. and Abrams, J.M. (2003) *Drosophila* p53 preserves genomic stability by regulating cell death. *Proc. Natl Acad. Sci. USA*, **100**, 4696–4701.
29. Akdemir, F., Christich, A., Sogame, N., Chapo, J. and Abrams, J.M. (2007) p53 directs focused genomic responses in *Drosophila*. *Oncogene*, **26**, 5184–5193.
30. Brodsky, M.H., Nordstrom, W., Tsang, G., Kwan, E., Rubin, G.M. and Abrams, J.M. (2000) *Drosophila* p53 binds a damage response element at the reaper locus. *Cell*, **101**, 103–113.
31. McEwen, D.G. and Peifer, M. (2005) Puckered, a *Drosophila* MAPK phosphatase, ensures cell viability by antagonizing JNK-induced apoptosis. *Development*, **132**, 3935–3946.
32. Madigan, J.P., Chotkowski, H.L. and Glaser, R.L. (2002) DNA double-strand break-induced phosphorylation of *Drosophila* histone variant H2Av helps prevent radiation-induced apoptosis. *Nucleic Acids Res.*, **30**, 3698–3705.
33. Peng, J.C. and Karpen, G.H. (2009) Heterochromatic genome stability requires regulators of histone H3 K9 methylation. *PLoS Genet.*, **5**, e1000435.
34. Boulton, S., Westman, B.J., Hutten, S., Boisvert, F.M. and Lamond, A.I. (2010) The nucleolus under stress. *Mol. Cell*, **40**, 216–227.
35. Reichow, S.L., Hama, T., Ferre-D'Amare, A.R. and Varani, G. (2007) The structure and function of small nucleolar ribonucleoproteins. *Nucleic Acids Res.*, **35**, 1452–1464.
36. Brodsky, M.H., Sekelsky, J.J., Tsang, G., Hawley, R.S. and Rubin, G.M. (2000) mus304 encodes a novel DNA damage checkpoint protein required during *Drosophila* development. *Genes Dev.*, **14**, 666–678.
37. Sancar, A., Lindsey-Boltz, L.A., Unsal-Kacmaz, K. and Linn, S. (2004) Molecular mechanisms of mammalian DNA repair and the DNA damage checkpoints. *Annu. Rev. Biochem.*, **73**, 39–85.
38. Aguilera, A. and Gomez-Gonzalez, B. (2008) Genome instability: a mechanistic view of its causes and consequences. *Nat. Rev. Genet.*, **9**, 204–217.
39. Malumbres, M. and Barbacid, M. (2009) Cell cycle, CDKs and cancer: a changing paradigm. *Nat. Rev. Cancer*, **9**, 153–166.
40. Okada, M., Akimaru, H., Hou, D.X., Takahashi, T. and Ishii, S. (2002) Myb controls G(2)/M progression by inducing cyclin B expression in the *Drosophila* eye imaginal disc. *EMBO J.*, **21**, 675–684.
41. Alvarez-Fernandez, M., Halim, V.A., Krenning, L., Aprelia, M., Mohammed, S., Heck, A.J. and Medema, R.H. (2010) Recovery from a DNA-damage-induced G2 arrest requires Cdk-dependent activation of FoxM1. *EMBO Rep.*, **11**, 452–458.
42. Tan, Y., Chen, Y., Yu, L., Zhu, H., Meng, X., Huang, X., Meng, L., Ding, M., Wang, Z. and Shan, L. (2010) Two-fold elevation of expression of FoxM1 transcription factor in mouse embryonic fibroblasts enhances cell cycle checkpoint activity by stimulating p21 and Chk1 transcription. *Cell Prolif.*, **43**, 494–504.
43. Mannefeld, M., Klassen, E. and Gaubatz, S. (2009) B-MYB is required for recovery from the DNA damage-induced G2 checkpoint in p53 mutant cells. *Cancer Res.*, **69**, 4073–4080.
44. Rubbi, C.P. and Milner, J. (2003) Disruption of the nucleolus mediates stabilization of p53 in response to DNA damage and other stresses. *EMBO J.*, **22**, 6068–6077.
45. Gatto, C.L. and Broadie, K. (2011) Fragile X mental retardation protein is required for programmed cell death and clearance of developmentally-transient peptidergic neurons. *Dev. Biol.*, **356**, 291–307.
46. Wan, L., Dockendorff, T.C., Jongens, T.A. and Dreyfuss, G. (2000) Characterization of dFMR1, a *Drosophila melanogaster* homolog of the fragile X mental retardation protein. *Mol. Cell Biol.*, **20**, 8536–8547.
47. Zhivotovsky, B. and Kroemer, G. (2004) Apoptosis and genomic instability. *Nat. Rev. Mol. Cell Biol.*, **5**, 752–762.
48. Casper, A.M., Nghiem, P., Arlt, M.F. and Glover, T.W. (2002) ATR regulates fragile site stability. *Cell*, **111**, 779–789.
49. Durkin, S.G. and Glover, T.W. (2007) Chromosome fragile sites. *Annu. Rev. Genet.*, **41**, 169–192.
50. Kumari, D., Somma, V., Nakamura, A.J., Bonner, W.M., D'Ambrosio, E. and Usdin, K. (2009) The role of DNA damage response pathways in chromosome fragility in Fragile X syndrome. *Nucleic Acids Res.*, **37**, 4385–4392.
51. Duncan, A.M. (1986) Enhanced sensitivity of lymphoblastoid cells from individuals carrying the mutation for the fragile X syndrome to the clastogenic effects of FUDR. *Mutat. Res.*, **173**, 201–205.
52. Li, S.Y. and Lin, J.K. (1990) Differential bleomycin susceptibility in cultured lymphocytes of fragile X patients and normal individuals. *Hum. Genet.*, **85**, 267–271.
53. Wang, T.S., Hsieh, L.J., Hsu, T.Y., Chung, C.H. and Li, S.Y. (2002) DNA damage and repair in lymphoblastoid cell lines from normal donors and fragile X syndrome patients. *Arch. Med. Res.*, **33**, 128–135.
54. Dockendorff, T.C., Su, H.S., McBride, S.M., Yang, Z., Choi, C.H., Siwicki, K.K., Sehgal, A. and Jongens, T.A. (2002) *Drosophila* lacking dfmr1 activity show defects in circadian output and fail to maintain courtship interest. *Neuron*, **34**, 973–984.
55. Nordstrom, W., Chen, P., Steller, H. and Abrams, J.M. (1996) Activation of the reaper gene during ectopic cell killing in *Drosophila*. *Dev. Biol.*, **180**, 213–226.
56. Yi, X., de Vries, H.I., Siudeja, K., Rana, A., Lemstra, W., Brunsting, J.F., Kok, R.M., Smulders, Y.M., Schaefer, M., Dijk, F. et al. (2009) Stw1 modifies chromatin compaction and is required to maintain DNA integrity in the presence of perturbed DNA replication. *Mol. Biol. Cell*, **20**, 983–994.
57. Yao, A., Jin, S., Li, X., Liu, Z., Ma, X., Tang, J. and Zhang, Y.Q. (2011) *Drosophila* FMRP regulates microtubule network formation and axonal transport of mitochondria. *Hum. Mol. Genet.*, **20**, 51–63.
58. Peritz, T., Zeng, F., Kannanayakal, T.J., Kilik, K., Eiriksdottir, E., Langel, U. and Eberwine, J. (2006) Immunoprecipitation of mRNA-protein complexes. *Nat. Protoc.*, **1**, 577–580.
59. Moon, N.S., Di Stefano, L., Morris, E.J., Patel, R., White, K. and Dyson, N.J. (2008) E2F and p53 induce Apoptosis Independently during *Drosophila* development but intersect in the context of DNA damage. *PLoS Genet.*, **4**, e1000153.
60. Pimpinelli, S., Bonaccorsi, S., Fanti, L. and Gatti, M. (2000) Preparation and analysis of *Drosophila* mitotic chromosomes. Sullivan, B., Ashburner, M. and Hawley, R.S. (eds), *Drosophila Protocols*. Cold Spring Harbor Laboratory Press, New York, pp. 3–23.